Electronic Supplementary Material (ESI) for ChemComm.

Controlling the Properties of both the Micellar and Gel Phase by Varying the Counterion in Functionalised-Dipeptide Systems

Kate McAulay,[a] Pedro Agís Ucha,[a,b] Han Wang,[c] Ana M. Fuentes-Caparrós,[a] Lisa Thomson,[a] Osama Maklad,[d] Nikul Khunti,[e] Nathan Cowieson,[e] Matthew Wallace,[f] Honggang Cui,[c] Robert J. Poole,[d] Annela Seddon,[g,h] and Dave J. Adams[a,*]

[a] School of Chemistry, University of Glasgow, Glasgow, G12 8QQ, U.K.

[b] Department of Chemical Engineering, Faculty of Sciences, 18071 Granada, Spain

[c] Department of Chemical and Biomolecular Engineering, Whiting School of Engineering, Johns Hopkins University, 3400 North Charles Street, Baltimore, MD 21218, USA

[d] School of Engineering, University of Liverpool, Liverpool, L69 3GH, U.K.

[e] Diamond Light Source Ltd, Harwell Science and Innovation Campus, Didcot, OX11 0QX, U.K.

[f] School of Pharmacy, University of East Anglia, Norwich Research Park, Norwich, NR4 7TJ, U.K.

[g] School of Physics, HH Wills Physics Laboratory, Tyndall Avenue, University of Bristol, Bristol, BS8 1TL, U.K.

[h] Bristol Centre for Functional Nanomaterials, HH Wills Physics Laboratory, Tyndall Avenue, University of Bristol, Bristol, BS8 1TL, U.K.

Supporting Information

1. Experimental Details

Materials The gelators used in this study were synthesised as reported previously.[1] All other chemicals were purchased from Sigma Aldrich. Deionised water was used throughout.

Stock Solutions Gelator stock solutions (10 mg/mL) were prepared by dissolving the gelator in deionised water with the addition of 1 molar equivalent of base (added from a 0.1 M solution of the base). The bases used were as follows: sodium hydroxide (NaOH, ≥ 98 %), lithium hydroxide (LiOH, ≥ 98 %), potassium hydroxide (KOH, ≥ 99.97%), cesium hydroxide hydrate ($CsOH.xH_2O$, ≥ 99.5 %), rubidium hydroxide (RbOH, 50 wt. % solution in H_2O, 99.9 %) and tetrabutylammonium hydroxide ((TBAOH; $CH_3CH_2CH_2CH_2)_4NOH$, 40 wt. % solution in H_2O). To prepare the stock solutions, 500 mg of 2NapFF was suspended in 38 mL of H_2O, and then 12 mL of a 0.1 M aqueous solution of the base added. The solutions were stirred at 1000 rpm overnight to ensure complete dissolution of the gelator. Next, the pH of each solution was measured and adjusted, if needed, to pH 11 ± 0.1 with the corresponding base.

Gel Samples. Gel samples were prepared in 7 mL Sterlin vials (by the addition of 2 mL gelator stock solution to glucono-δ-lactone (GdL, ≥ 99 %, 16 mg, 4.46 molar equivalents relative to the 2NapFF – we have previously found that this ratio provides suitable kinetics of gelation[1, 2]). The vials were gently rotated by hand to ensure completed dissolution of GdL and left to stand quiescently overnight. Rheology data was collected 18 hours after the addition of GdL.

In the case of samples for the temperature sweep measurements, the gels were prepared in aluminium cups to ensure good heat transfer between the sample and rheometer. The samples were sealed with parafilm to prevent evaporation overnight.

Heat-Cool Cycles. The solutions were heated to 50 °C for 30 minutes before being cooled to room temperature. On standing, the samples were noticeably more viscous.

pH Measurements. All pH measurements were performed using a FC200 pH probe (HANNA Instruments) with a 6 mm x 10 mm conical tip. The accuracy of the pH measurements is quoted as ± 0.1.

pK_a Measurements. The apparent pK_a values of 2NapFF solutions at a concentration of 10 mg/mL were determined *via* titration by the addition of aliquots of a 0.1 M HCl solution. The pH values were recorded after each addition of acid when a stable pH value was achieved. To prevent gel formation, the solutions were constantly stirred to ensure the sample was liquid throughout the entire experiment.

Rheology. Rheological measurements were carried out using Anton Paar Physica MCR301 and MCR101 Rheometers.

Time Sweeps. 2 mL of the 10 mg/mL stock solutions were added to predetermined masses of GdL (Table S4). The vial was gently swirled to ensure the complete dissolution of GdL. Next, 1 mL of the stock and GdL solution was pipetted on to the rheometer flat plat using a 1 mL pipette tip. Time sweep measurements were performed at 25 °C using a using a 50 mm sandblasted parallel plate and a measuring gap of 0.8 mm. A constant frequency of 10 rad s^{-1} and a strain of 0.5 % was applied. The storage (G') and loss (G") moduli were measured over time for 16 hours.

Frequency and Strain Sweeps. A cup and vane (ST10-4V-8.8/97.5-SN42404) system, with a measuring gap of 1.8 mm, was used for frequency and strain sweeps so that measurements could be directly performed in the 7 mL Sterilin vials. Frequency sweeps were performed from 1 rad s^{-1} to 100 rad s^{-1} at a constant strain of 0.5 %. Strain sweeps were performed from 0.1 % to 1000 % at a frequency of 10 rad s^{-1}. This method ensured that 0.5 % strain was in the viscoelastic region required for measuring the frequency sweep.

Temperature Sweeps. Temperature sweep measurements were performed using a strain of 0.5 %, frequency of 10 rad s^{-1} and a measuring gap of 1 mm. The samples were heated from 20 °C to 90 °C then cooled from 90 °C to 20 °C using a ramp rate of 1 °C min^{-1}. The cup and vane system was using with an aluminium cup to ensure good heat transfer.

Viscosity Measurements. A 50 mm cone and plate system was used at 25 °C. The gap distance between two plates used was 0.1 mm. The samples were poured on to the rheometer plate to minimise shear effects. The viscosity of each solution was recorded under rotation shear rate varying from 0.1 to 1000 s^{-1}.

Extensional Viscosity. A capillary breakup extensional rheometer (CaBER), made by Haake Thermo Scientific, was used to quantify the change of the extensional viscosity of the solutions before and after the heat/cool cycle. In this experiment, a liquid bridge of 2 mm in length is formed in a cylindrical shape between two circular discs of 4 mm in diameter. These two discs are rapidly pulled apart (~ 50 ms) until a final height of (~7 mm) and an unstable filament is formed with continuous decrease in diameter under the combined effect of surface tension and viscoelastic extensional forces until it finally breaks.[3] The diameter of the filament (D) is tracked as a function of time (t) using a high speed camera (100-500 frames/s) and a MATLAB® script applying Canny edge detection method[4, 5] which returns a binary image containing ones where the function finds edges in the input image and zeros elsewhere. Although the filament diameter data can be post-processed into an (apparent) extensional viscosity, the standard method to quantify extensional effects[6] is via an exponential fit to the filament diameter as a function of time in the elastocapillary regime to determine a characteristic relaxation time (λ; more correctly a characteristic time for extensional stress growth).

Confocal Microscopy. A Zeiss LSM 710 confocal microscope was used to take confocal images. The objective used was a LD EC Epiplan NEUFLUAR 50x (0,55 DIC). The samples were stained with 2 µL/mL of a 0.1 wt % Nile Blue solution and excited using a HeNe laser at 634 nm. 1 mL samples were prepared in vials with GdL after complete dissolution of GdL 400 µL of the sample was pipetted into the centre of the confocal dishes. Tissue saturated with deionized water was carefully wrapped inside the dish with no contact between the tissue and the sample, to ensure a humid environment to prevent evaporation of the sample. Next the confocal dish was sealed with parafilm and left overnight to gel before analysis.

Cryo-TEM. Cryogenic TEM imaging was performed using a FEI Tecnai 12 TWIN Transmission Electron Microscope, operating at 100 kV. The solutions were immediately diluted five times with water to reduce their viscosity and 6 µL of sample solution was placed on a holey carbon film supported on a TEM copper grid (Electron Microscopy Services, Hatfield, PA). All the TEM grids used for cryo-TEM imaging were treated with plasma air to render the lacey carbon film hydrophilic. A thin film of the sample solution was produced using the Vitrobot with a controlled humidity chamber (FEI). After loading of the sample solution, the lacey carbon grid was blotted using preset parameters and plunged instantly into a liquid ethane reservoir precooled by liquid nitrogen. The vitrified samples were then transferred to a cryo-holder and cryo-transfer stage, which was cooled by liquid nitrogen. To prevent sublimation of vitreous water, the cryo-holder temperature was maintained below −170 °C during the imaging process. All images were recorded by a SIS Megaview III wide-angle CCD camera.

Optical Microscopy. Optical microscope images were collected using a Nikon Eclipse LV100 microscope with a Nikon Plan ELWD 20x/0.45 lens attached to an Infinity2-1C camera. Images were collected under polarised and non-polarised light.

NMR. The experiments are based on previous work, where we have shown that 2NapFF aligns in a magnetic field,[7] which leads to the residual quadrupolar coupling effects seen here. This alignment occurs in a 5 mm NMR tube once inserted into the spectrometer and is field dependent.[7] NMR spectra were acquired using a Bruker 400 MHz (^{1}H) spectrometer equipped with a broad band probe. ^{1}H spectra were acquired using the perfect echo WATERGATE sequence of Adams et al.[8] incorporating the double echo W5 sequence of Liu et al.[9] The acquisition time was set at 2.5 s. The delay between successive hard pulses of the selective pulse train was set at 333 µs corresponding to a 3000 Hz spacing between the null points. The relaxation delay was set at 1 s. ^{2}H spectra were acquired *via* the lock channel using a 90 degree pulse. 128 scans were acquired with an acquisition time of 2 s, a relaxation delay of

0.2 s and a sweep width of 10 ppm. ^{7}Li spectra were acquired in 64 scans using a 30 degree pulse, a signal acquisition time of 3.1 s, a relaxation delay of 10 s and a sweep width of 68 ppm. ^{23}Na spectra were acquired in 256 scans using a 90 degree pulse, a signal acquisition time of 0.3 s, a relaxation delay of 0.1 s and a sweep width of 120 ppm. ^{39}K spectra were acquired using the aring sequence (π/2- π/2- π/2-aquire) in order to supress acoustic ringing effects in our probe. 4096 (Figure S1a, lower) and 2048 scans (Figure 3) were acquired with a signal acquisition time of 0.3 s, a relaxation delay of 0.1 s and a sweep width of 90 ppm. ^{87}Rb spectra were acquired in 4096 (Figure 3) and 2048 (Figure S4) scans using a 90 degree pulse, a signal acquisition time of 0.1 s, a relaxation delay of 0.1 s and a sweep width of 300 ppm. ^{133}Cs spectra were acquired using the aring sequence in 32 scans with 4 dummy scans using a signal acquisition time of 3 s, a relaxation delay of 10 s and a sweep width of 202 ppm.

Small Angle X-Ray Scattering (SAXS). SAXS was obtained at beamline B21 at the Diamond Light Source. This beamline operates at a fixed energy of 12.4 keV and a camera length of 4.014 m, resulting in a Q range of 0.004 – 0.44 Å-1. The samples were manually loaded into borosilicate glass capillaries (Capillary Tube Supplies UK). Measurement times were 15 s for each sample. 14 frames were acquired and averaged. Data were processed using DAWN[10] and a water background was subtracted as a 2D image within the processing pipeline.

Additional data were collected on a SAXSLAB Ganesha 300XL instrument. 70uL of the solutions as prepared above in H_2O were transferred to a borosilicate glass capillary (Capillary Tube Supplies UK), sealed, and measured for 3600 s in a Q range of 0.007 - 0.25 $Å^{-1}$. Gels were prepared by addition of GdL to the solution in 10mL glass vials before transfer to the capillary, sealed and allowed to gel overnight. Data were corrected for transmission, absolute intensity and capillary width in SAXSGUI.

All data were fitted using SASView 4.0.[11] As the length of the scattering objects falls outside of the Q range for the experiment, an arbitrarily long length was introduced into the model and not allowed to refine.

2. Viscosity Data

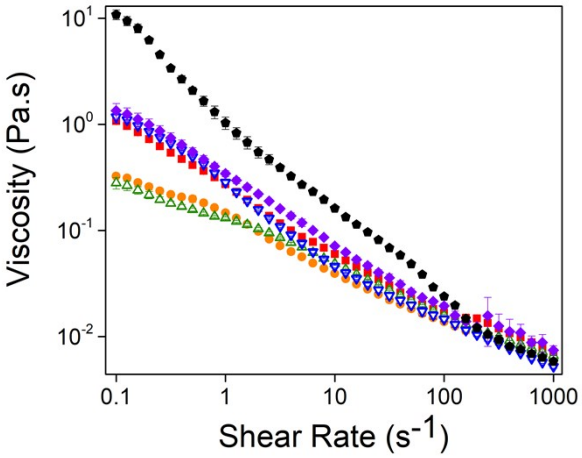

Figure S1. Shear viscosity measurements for solutions prepared at 10 mg/mL using (■) Li-2NapFF, (△) Na-2NapFF, (●) K-2NapFF (▽) Rb-2NapFF, (◆) Cs-2NapFF and (⬟) TBA-2NapFF.

3. Cryo-TEM images

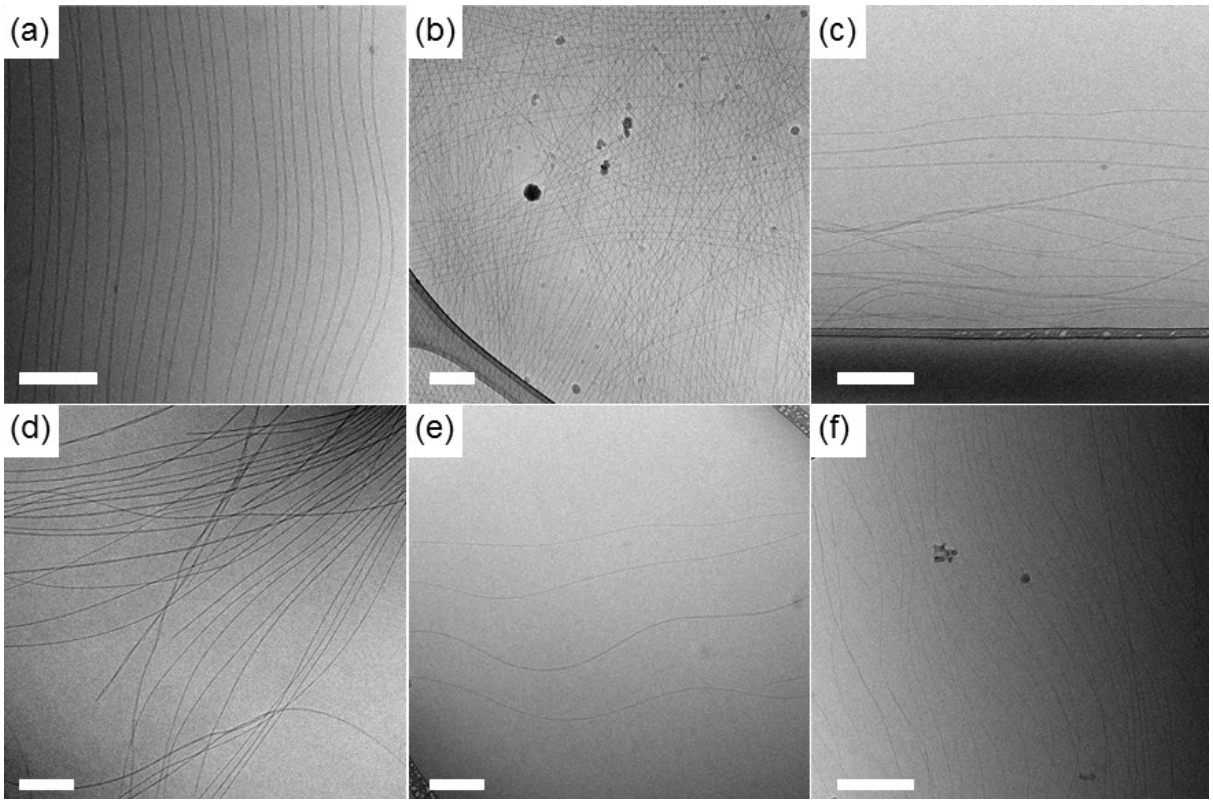

Figure S2. Cryo-TEM images of (a) Li-2NapFF; (b) Na-2NapFF; (c) K-2NapFF; (d) Rb-2NapFF; (e) Cs-2NapFF; (f) TBA-2NapFF. In all cases, the scale bar represents 200 nm.

4. Small Angle X-ray Scattering

The data were fitted to models available in SASView. Where necessary, models were combined using the "Easy Sum/Multi(p1, p2) editor" in the SasView software. A scattering length density of 14.196 x 10^{-6} Å^{-2} was used for the 2NapFF and a scattering length density of 9.469 x 10^{-6} Å^{-2} was used for the solvent. The SLDs were calculated using the software available from NIST.[12]

	Li-2NapFF	Na-2NapFF	K-2NapFF	Rb-2NapFF	Cs-2NapFF	TBA-2NapFF
Model	Flexible elliptical cylinder	Flexible cylinder	Flexible cylinder	Flexible cylinder	Flexible cylinder	Flexible cylinder + PL
Scale	$2.1x10^{-6}$± $3.8x10^{-9}$	0.016± 0.0001	$4.2x10^{-6}$± $3.0x10^{-9}$	$5.0x10^{-6}$± $7.4x10^{-9}$	$6.3x10^{-6}$± $2.6x10^{-9}$	$2.2x10^{-7}$± $4.2x10^{-9}$
Background	$3.9x10^{-5}$± $3.9x10^{-7}$	0.0060± 0.0002	$5.3x10^{-5}$ ±$3.0x10^{-7}$	$3.6x10^{-5}$± $4.1x10^{-7}$	$5.8x10^{-5}$± $2.8x10^{-7}$	$4.9x10^{-6}$± $1.9x10^{-7}$
Radius / Å	30.95± 0.05	42.84± 0.27	42.72± 0.02	40.91± 0.04	46.57± 0.01	14.18± 0.13
Axis ratio	2.03					
Kuhn length / Å	865.4± 16.6	771.2± 116.3	585.6± 6.7	412.3± 0.0008	419.2± 0.83	214.3± 10.47
Length / Å	>1000	>3000	>3000	>3000	>3000	>3000
Polydispersity				0.22± 0.001	0.12± 0.001	
Power Law Scale						$1.58x10^{-8}$ ±$3.1x10^{-10}$
Power Law						2.3
Chi Squared	14.70	1.14	4.83	5.52	9.12	4.99

Table S1. Fitting parameters for SAXS data collected for solutions at high pH.

SAXS was performed on the gels formed from each high pH solution (it was found to be extremely difficult to probe the gels using cryo-TEM due to their stiffness). The scattering patterns and fits are shown in Figure S3. Na-2NapFF forms a gel which can be fitted to a flexible elliptical cylinder model, as we have previously shown.[13] The data for the remaining samples also fit to a flexible elliptical cylinder model with the addition of a power law. The fact that regardless of salt, all gels are the result of the formation of similar structures is evidence that the mechanism of gelation is comparable in all cases and is not inherently affected by the salt and kinetics of gelation. In solution, Li-NapFF was best fit to a flexible elliptical cylinder to account for its helicity (see above). The gel of Li-2NapFF also fits to a flexible elliptical cylinder with an increased minor radius of 3.6 nm and a decreased major radius of 5.4 nm. Whilst in previous work on Na-2NapFF we have attributed the growth of the gel network to the lateral aggregation of cylinders during the gelation process (and thus an increase in the lateral dimension), with Li-2NapFF the starting structure is significantly different. Comparison of the cross-sectional area of the scattering object before and after gelation of Li-2NapFF shows no significant increase in size (60.381 nm^2 in solution compared to 61.073 nm^2 in the gel) which may be indicative that the helical structure formed at high pH cannot pack as effectively as the cylinders formed in the presence of other salts, leading to a less dramatic structural change. Gels formed from K-2NapFF, Rb-2NapFF and Cs-2NapFF have similar minor radii (2.9 nm, 3.1 nm, 3.0 nm respectively). Their major radii increase with an increase in the size of the cation, with K-2NapFF having a major radius of 4.1 nm, Rb-2NapFF having a major radius of 5.9 nm and Cs-2NapFF measured at 6.6 nm. Interestingly, the minor radius of Na-2NapFF follows this trend with a value of 2.5 nm, however the major radius is larger (5.0 nm) than would be expected if the lateral

association was simply related to the size of the cation. This is suggestive that the salt is affecting the degree of lateral aggregation in the sample, with larger counterions promoting the formation of more aggregated structures. However, for the gels formed from TBA-2NapFF, this approximation breaks down as the gel minor axis is still comparatively small at 1.6 nm in radius and the major axis is 3.0 nm. TBA-2NapFF in solution has a much smaller structure, so it is perhaps unsurprising that the structure formed by the gel is also smaller than that of those formed by the other cations. These data show that the micellar aggregates formed at high pH directly link to the structures present in the gel phase.

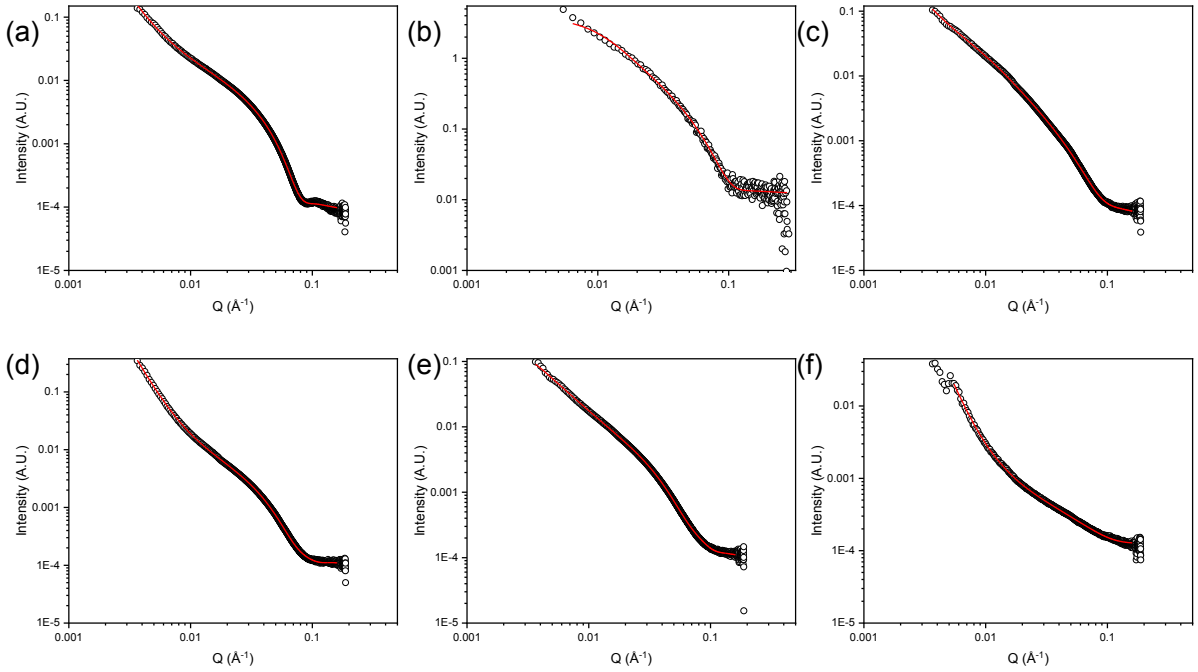

Figure S3. Experimental data (black open circles) and fits (red line) for gels formed from (a) Li-2NapFF; (b) Na-2NapFF; (c) K-2NapFF; (d) Rb-2NapFF; (e) Cs-2NapFF; (f) TBA-2NapFF. The parameters from the fits are shown in Table S2.

	Li-2NapFF	Na-2NapFF	K-2NapFF	Rb-2NapFF	Cs-2NapFF	TBA-2NapFF
Model	Flexible elliptical cylinder + PL	Flexible elliptical cylinder	Flexible elliptical cylinder + PL	Flexible elliptical cylinder + PL	Flexible elliptical cylinder + PL	Flexible elliptical cylinder + PL
Scale	2.49×10^{-6} $\pm3.6\times10^{-9}$	0.00060± 2.9x10^{-5}	1.24×10^{-6} $\pm1.4\times10^{-8}$	2.73×10^{-6} $\pm4.7\times10^{-9}$	2.19×10^{-6} $\pm1.3\times10^{-8}$	1.026×10^{-6} $\pm4.2\times10^{-8}$
Background	9.20×10^{-5} ± 2.5×10^{-7}	0.013± 0.0002	6.90×10^{-5} $\pm1.8\times10^{-6}$	0.0001± 2.5×10^{-7}	9.66×10^{-5} $\pm1.8\times10^{-6}$	0.0001± 1.7×10^{-6}
Radius / Å	35.90± 0.04	24.93± 0.72	29.40± 0.86	30.72± 0.02	29.73± 0.21	16.20± 0.1
Axis ratio	1.52± 0.003	2.07± 0.08	1.40± 0.06	1.92± 0.002	2.19± 0.02	1.87± 0.01
Kuhn length / Å	709.3 ± 36.60	247.3± 0.01	32.5± 0.35	1326± 31.5	319.3± 7.5	264.6± 0.004
Length / Å	>3000	>1000	>3000	>3000	>3000	>3000
Power Law Scale	1.02×10^{-10} $\pm3.1\times10^{-11}$		1.47×10^{-7} $\pm2.2\times10^{-8}$	2.47×10^{-10} $\pm1.7\times10^{-11}$	2.30×10^{-7} $\pm3.6\times10^{-8}$	2.28×10^{-12} ±8.7x10-^{14}
Power Law	3.6± 0.05		2.4± 0.03	3.7± 0.02	2.1± 0.29	4.4± 0.008
Chi Squared	5.98	1.56	10.34	6.34	4.00	1.87

Table S2. Fitting parameters for SAXS data collected for gels.

5. NMR Studies

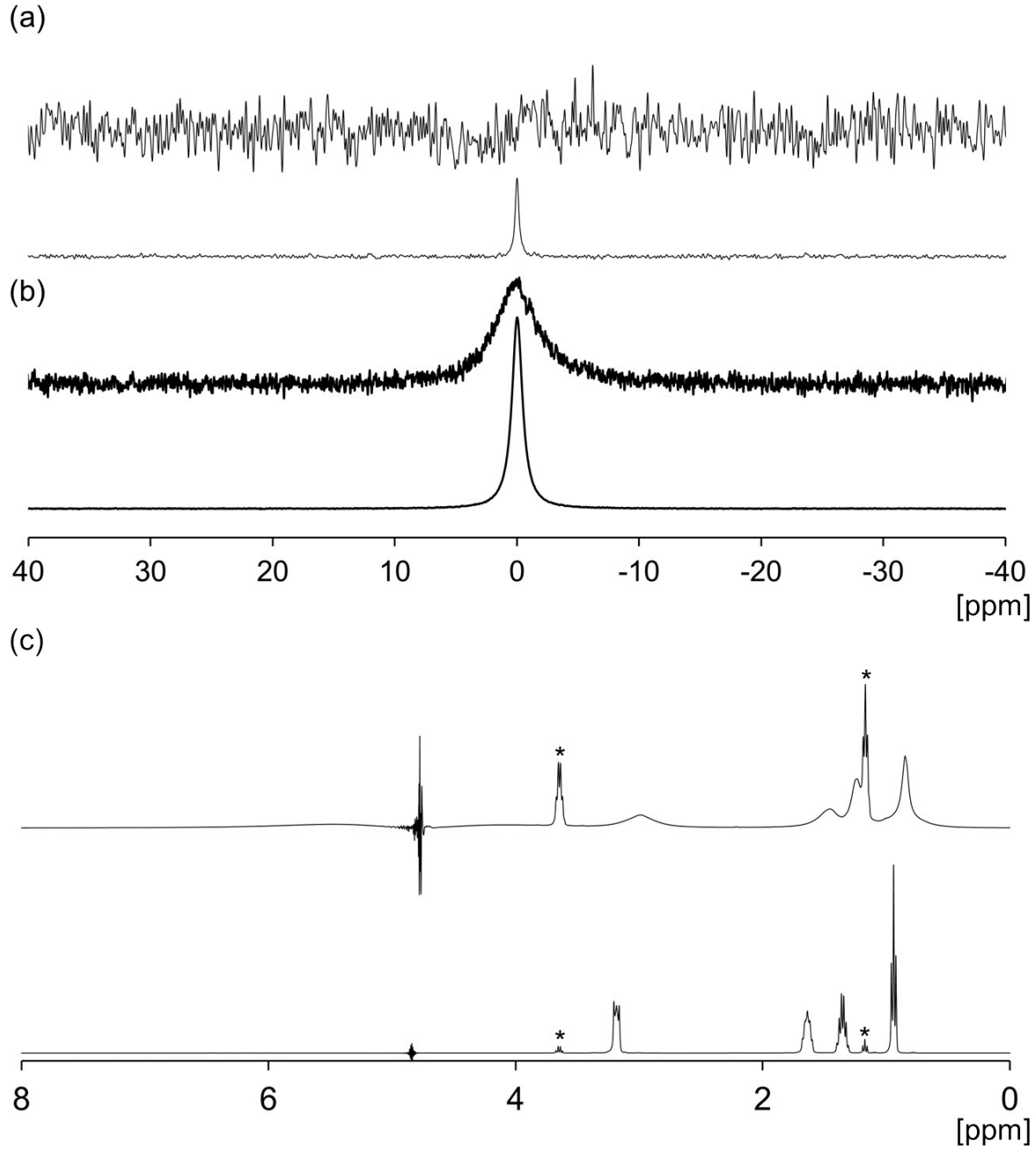

Figure S4. NMR spectra acquired in 10 mg/mL samples of 2NapFF (upper) and in 0.1 M solution of hydroxide (lower). (a) ^{39}K, (b) ^{87}Rb and TBA (^{1}H, c). The peaks marked * correspond to 2 µL/mL ethanol added for comparison with the TBA resonances. ^{1}H spectra were calibrated to 1.17 ppm (CH_3, ethanol). All ^{39}K and ^{87}Rb resonances were set to 0 ppm to allow comparison of relative linewidths. No ^{87}Rb quadrupolar satellites could be detected in the 2NapFF sample.

6. pH Studies

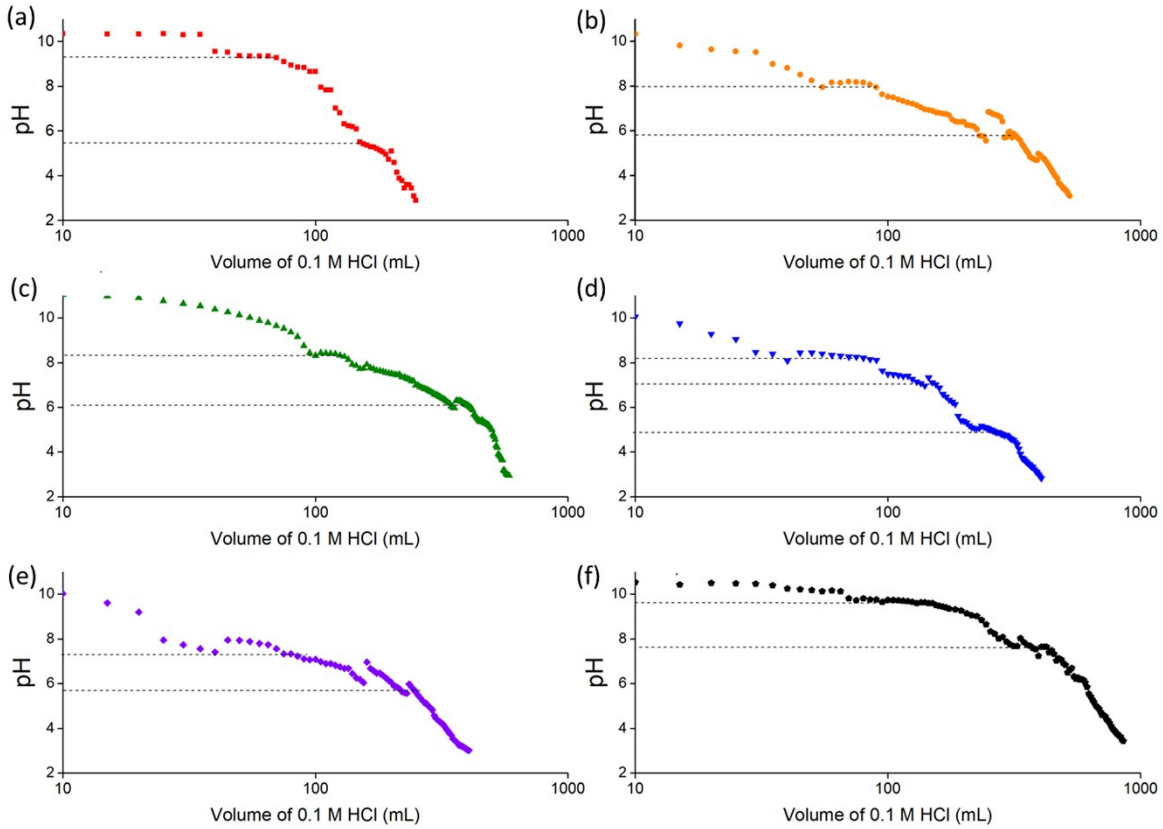

Figure S5. pK_a titrations for 2NapFF solutions at a concentration of 10 mg/mL for (a) Li-2NapFF, (b) Na-2NapFF, (c) K-2NapFF, (d) Rb-2NapFF, (e) Cs-2NapFF and (f) TBA-2NapFF. The dashed lines show extrapolated values for the apparent pK_a.

Solution	pK_a 1 (pH)	pK_a 2 (pH)
Li-2NapFF	9.3	6.0
Na-2NapFF	8.0	5.5
K-2NapFF	8.3	6.0
Rb-2NapFF	8.3	7.1
Cs-2NapFF	7.3	5.7
TBA-2NapFF	9.6	7.6

Table S3. pH values from pK_a titrations for 2NapFF solutions at a concentration of 10 mg/mL. NB, there is a third apparent pK_a for the Rb-2NapFF at 4.9.

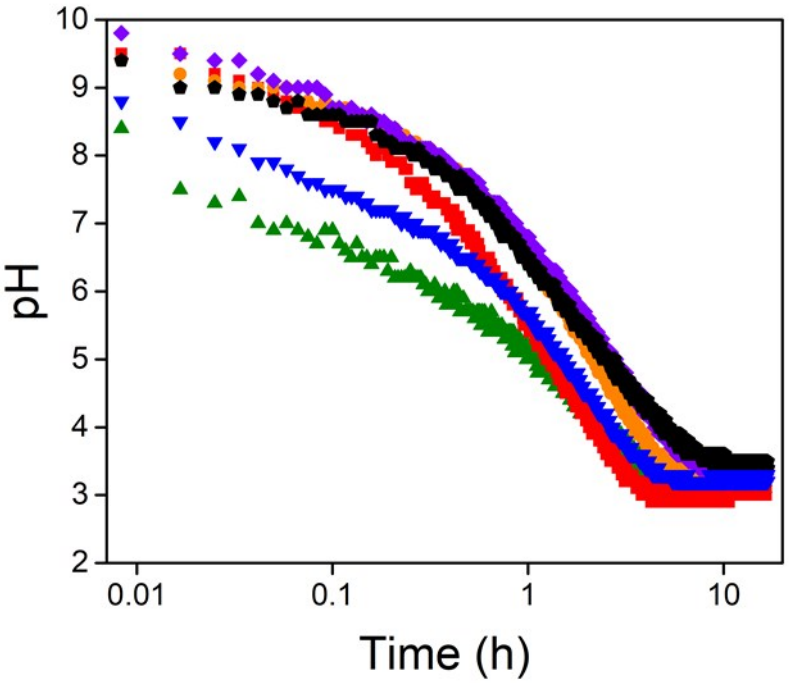

Figure S6. Change in pH with time post-addition of GdL to solutions of 2NapFF prepared using different metal hydroxides with 16 mg GdL. Data are shown for 2NapFF-Li(■), 2NapFF-K(●), 2NapFF-Na(▲), 2NapFF-Rb (▼), 2NapFF-Cs (◆) and 2NapFF-TBA (⬟).

7. Rheology

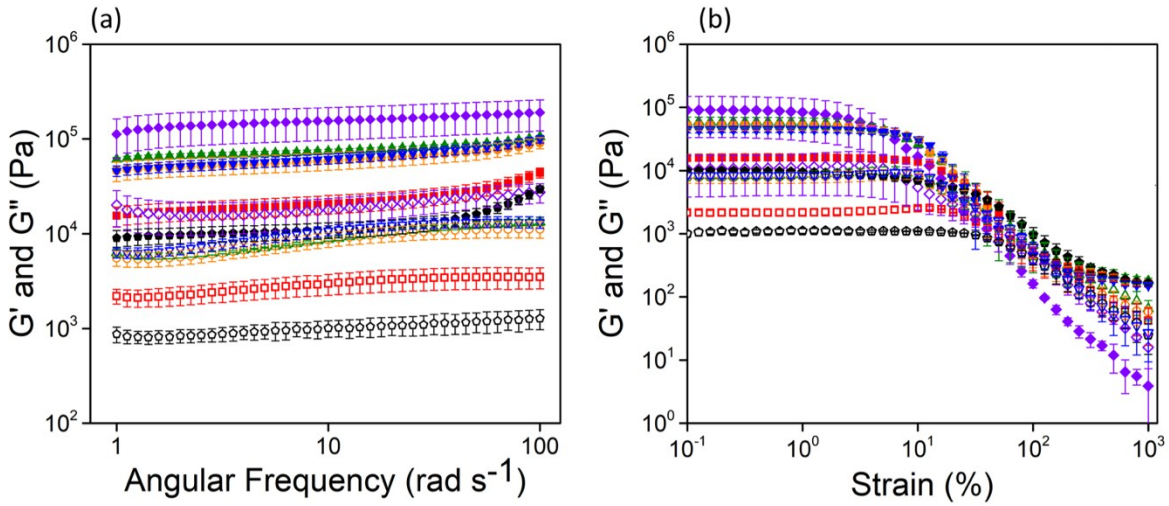

Figure S7. (a) Frequency sweeps and (b) strain sweeps for 2NapFF gels at a concentration of 10 mg/mL formed by addition of GdL to stock solutions prepared using (■) LiOH, (●) KOH, (▲) NaOH, (▼) RbOH, (◆) CsOH and (⬟) TBAOH. Open symbols represent G' and closed symbols represent G".

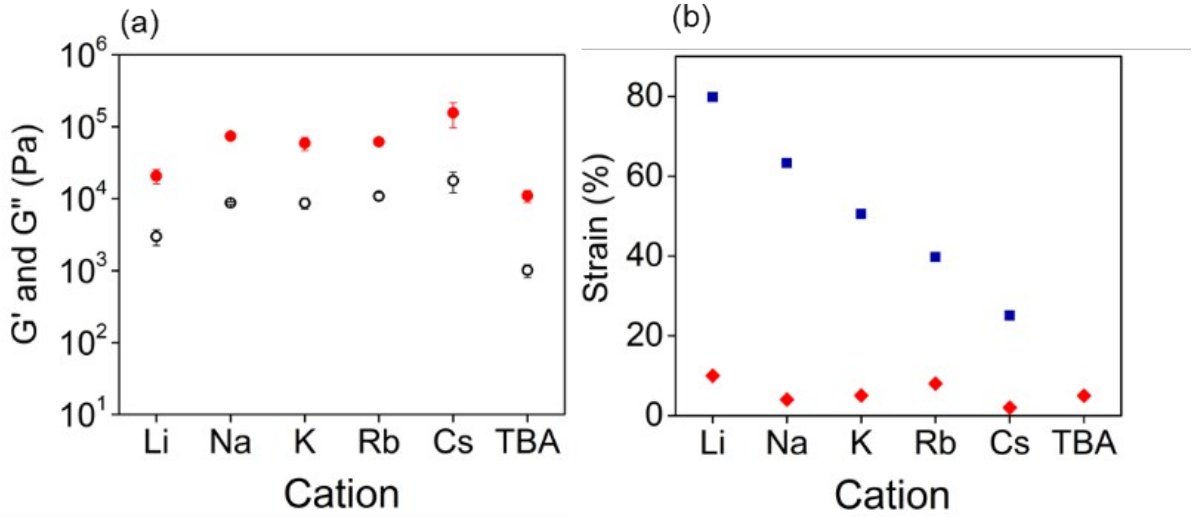

Figure S8. Rheology for gels Li-2NapFF, Na-2NapFF, K-2NapFF, Rb-2NapFF, Cs-2NapFF and TBA-2NapFF; a) Frequency sweep values at 10 rad/s for all gels G′ (●) and G″ (○) and b) Break points from strain sweeps G′ equals G″ (■) and deviation from linearity (◆).

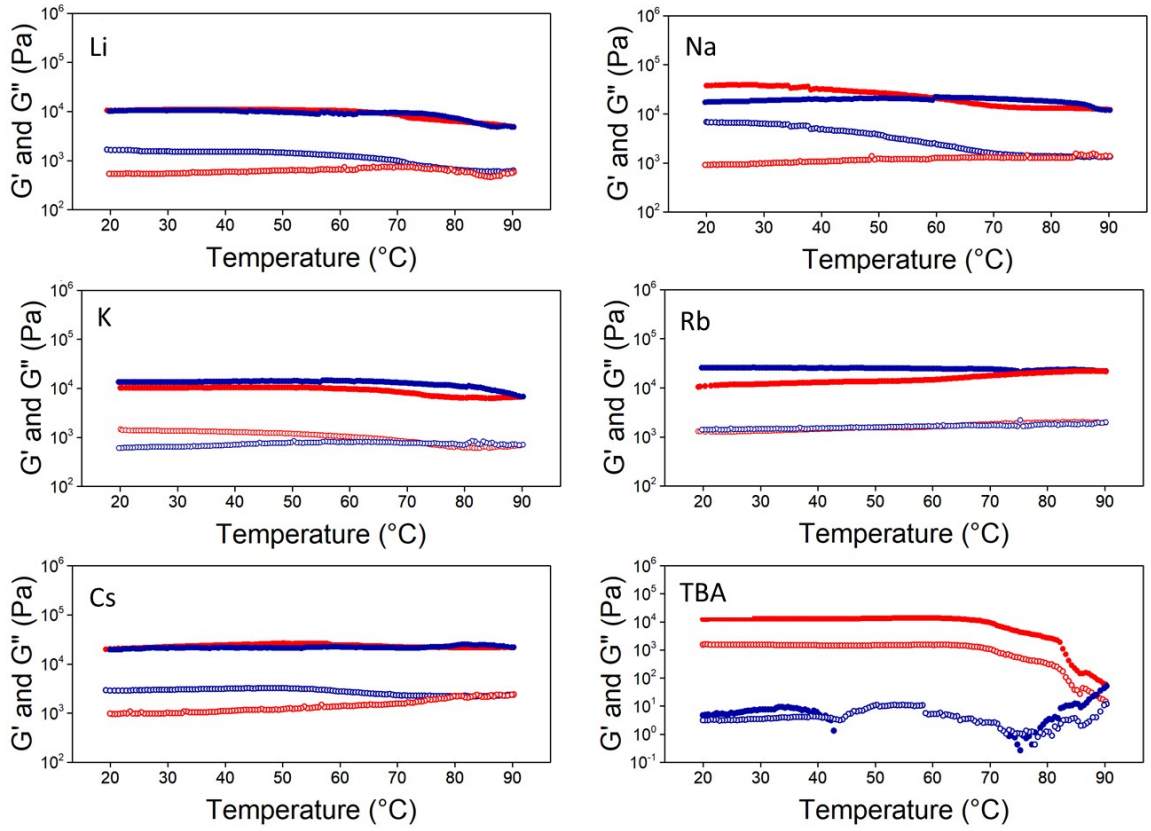

Figure S9. Temperature Sweeps for 2NapFF gels formed at a concentration of 10 mg/mL formed by addition of GdL to stock solutions prepared using different metal hydroxides. Temperature swept from 20 – 90 °C (red) then cooled from 90 – 20 °C (blue). Open symbols represent G' and closed symbols represent G".

9. References

1. L. Chen, S. Revel, K. Morris, L. C. Serpell and D. J. Adams, *Langmuir*, 2010, **26**, 13466-13471.
2. D. J. Adams, M. F. Butler, W. J. Frith, M. Kirkland, L. Mullen and P. Sanderson, *Soft Matter*, 2009, **5**, 1856-1862.
3. E. Rodd Lucy, P. Scott Timothy, J. Cooper-White Justin and H. McKinley Gareth, *Journal*, 2005, **15**, 12.
4. J. Canny, *IEEE Transactions on Pattern Analysis and Machine Intelligence*, 1986, **PAMI-8**, 679-698.
5. J. R. Parker, *Algorithms for Image Processing and Computer Vision*, Wiley Publishing, 2010.
6. L. Campo-Deaño and C. Clasen, *Journal of Non-Newtonian Fluid Mechanics*, 2010, **165**, 1688-1699.
7. M. Wallace, A. Z. Cardoso, W. J. Frith, J. A. Iggo and D. J. Adams, *Chemistry – A European Journal*, 2014, **20**, 16484-16487.
8. R. W. Adams, C. M. Holroyd, J. A. Aguilar, M. Nilsson and G. A. Morris, *Chemical Communications*, 2013, **49**, 358-360.
9. M. Liu, X.-a. Mao, C. Ye, H. Huang, J. K. Nicholson and J. C. Lindon, *Journal of Magnetic Resonance*, 1998, **132**, 125-129.
10. J. Filik, A. W. Ashton, P. C. Y. Chang, P. A. Chater, S. J. Day, M. Drakopoulos, M. W. Gerring, M. L. Hart, O. V. Magdysyuk, S. Michalik, A. Smith, C. C. Tang, N. J. Terrill, M. T. Wharmby and H. Wilhelm, *Journal of Applied Crystallography*, 2017, **50**, 959-966.
11. www.sasview.org/.
12. https://www.ncnr.nist.gov/resources/activation/.
13. E. R. Draper, B. Dietrich, K. McAulay, C. Brasnett, H. Abdizadeh, I. Patmanidis, S. J. Marrink, H. Su, H. Cui, R. Schweins, A. Seddon and D. J. Adams, *Matter*, 2020, DOI: https://doi.org/10.1016/j.matt.2019.12.028.